A novel flexible barrier for landslide impact in centrifuge

C. W. W. NG*, D. SONG*, C. E. CHOI*, R. C. H. KOO† and J. S. H. KWAN†

Experimental investigations aimed at understanding the impact mechanism of debris-resisting flexible barriers have been hindered by limitations associated with small-scale modelling and poor temporal predictability of real landslide debris events. The geotechnical centrifuge provides a means to simulate landslide impact by scaling the flow volume, impact energy and stress state appropriately. Nonetheless, a technical challenge remains in simulating large non-linear deformation of flexible barriers observed in a prototype. In this letter, the development and verification of a novel model flexible barrier for centrifuge testing are described. This model barrier consists of a series of spring elements to simplify the complex loading behaviour and to capture the key bilinear load–displacement response of a prototype flexible barrier. By measuring the dynamic response of barrier cables, no obvious peak impact load was captured. The shear strength of dry granular flow results in an attenuating pileup impact mechanism. It is apparent that the geometry of the debris front has a strong influence on impact response. In addition, as debris impacts and deposits behind the barrier, the debris–barrier interaction results in an active failure mode of the deposited material, which is a surrogate of reduced pressure acting on the barrier.

INTRODUCTION
The use of flexible barriers to arrest landslides and avalanches is becoming more prevalent around the world due to its large deformation, which makes it suitable to arrest dynamic impact loads (Volkwein *et al.*, 2011; Kwan *et al.*, 2014). Despite the engineering value of flexible barriers, their impact mechanisms and performance in practice are currently not well understood given a lack of high-quality physical data.

As soil is a stress-dependent material, centrifuge modelling ensures that the prototype stress states can be reasonably approximated by elevating the centrifugal gravitational field in a test. Furthermore, the dimensionless groups proposed by Iverson (1997, 2015) are also required to ensure that the relative ratios between selected stresses in the centrifuge model match those in the prototype. It is worthwhile to note that Bowman *et al.* (2010) carried out a series of centrifuge tests and demonstrated that the centrifuge offers a closer representation of the dimensionless groups for natural events compared with small-scale 1*g* modelling. However, modelling large and non-linear deformation of flexible barriers still remains a technical challenge. This study introduces the development and performance of a novel flexible barrier model for centrifuge modelling.

LOADING BEHAVIOUR OF FLEXIBLE BARRIERS
A flexible barrier relies on complex interactions between individual structural components to attenuate the dynamic impact. These components consist of the net, horizontal cables, energy-dissipating elements and posts. When debris impacts the barrier net, forces are transferred to the horizontal cables, which in turn activate the energy-dissipating elements (Wendeler *et al.*, 2007). Energy-dissipating elements rely on large elasto-plastic deformation of structural elements to attenuate the induced impact pressure. To capture the complex prototype behaviour for centrifuge modelling, it is imperative to simplify and model an equivalent model barrier by capturing the load–displacement behaviour of the energy-dissipating elements.

Figure 1 shows the measured static loading behaviour of an energy-dissipating element of a prototype barrier. The performance of the energy-dissipating element has been investigated by way of field monitoring and compared with the numerical simulations (Wendeler *et al.*, 2006, 2007; Zhou *et al.*, 2011; Chan *et al.*, 2012). The prototype loading behaviour exhibits a stiff response initially and then a softer response once the energy-dissipating element is activated. It is quite clear that a bilinear relationship appears to be appropriate to simplify and characterise the overall loading behaviour of a prototype barrier. Details of the measured loading behaviour of the newly developed model flexible barrier are discussed below.

DESIGN AND DEVELOPMENT OF A MODEL FLEXIBLE BARRIER
Scaling
The downslope debris motion is driven by the gravitational potential, and the velocity scale is $(gL)^{1/2}$, where L is the flow length. In centrifuge modelling, the gravitational acceleration increases N times and linear dimensions (e.g. L) reduce N times, resulting in a scale factor of unity for velocity (Chikatamarla *et al.*, 2006). Scaling of a model barrier relies on the physical process of debris–barrier interaction. Based on conservation of momentum, the impact pressure ($p \sim \rho v^2$) on the barrier is the same as that of the prototype, since both density (ρ) and velocity (v) have unity scale factors. The total impact force F on the barrier has the form

1
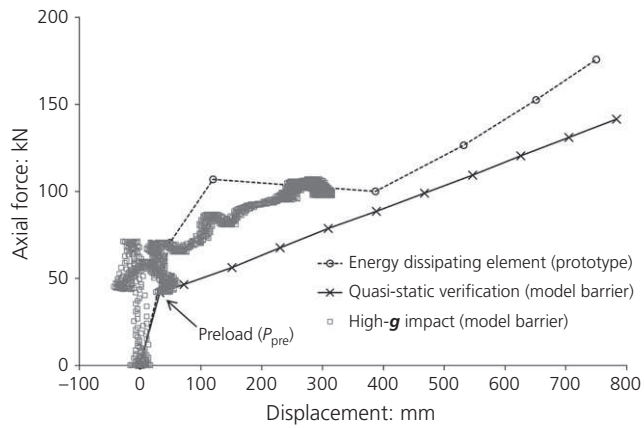
Fig. 1. Comparison of load–displacement behaviour for the horizontal cable. The 'quasi-static verification (model barrier)' and 'high-*g* impact (model barrier)' are measured in model scale and further scaled up to prototype scale by the scaling laws

Table 1. Summary of relevant scaling laws (Taylor, 1995)

Parameter	Dimension	Scaling law (model/prototype)
Gravity	L/T^2	N
Density	M/L^3	1
Length/displacement	L	$1/N$
Mass	M	$1/N^3$
Velocity	L/T	1
Stress	M/T^2L	1
Force	ML/T^2	$1/N^2$
Kinetic energy	ML^2/T^2	$1/N^3$
Inertial time	T	$1/N$

$F \sim \rho v^2 A$, where A is the impact area of the flexible barrier. Due to the reduced length scale, the impact area A has a scale factor of $1/N^2$, while the scaling of ρv^2 is unity, resulting in a scale factor of $1/N^2$ for the impact force (Chi *et al*., 2012).

The complex deformation in flexible barriers was simplified using a series of spring elements and the details are discussed later. Although springs with large elastic deformation are not commonly adopted in the centrifuge, the scaling of the displacement and loading behaviours of spring elements simply obey Hooke's law. This is reminiscent of adopting springs to model struts in a braced excavation (Nakai *et al*., 2007). In the impact process, the displacement and force of spring elements are scaled by $1/N$ and $1/N^2$ times, respectively. The relevant scaling laws are summarised in Table 1.

Spring element
Figures 2(a)–2(c) show the working mechanism, loading behaviour and schematic diagram of the spring element, respectively. Each spring element comprises two springs, a stiffer spring (k_1) and a softer spring (k_2), encased inside a cylindrical shell. The two springs housed within their own chambers are separated using a fixed separator. Each spring rests against an end plate and is initially in contact with the separator. The other end of the spring rests against the end of the cylindrical shell.

Initially, spring k_2 is preloaded to P_{pre} by inserting a spacer of a specified displacement between the end plate and the spring. If the tensile force applied to the spring element
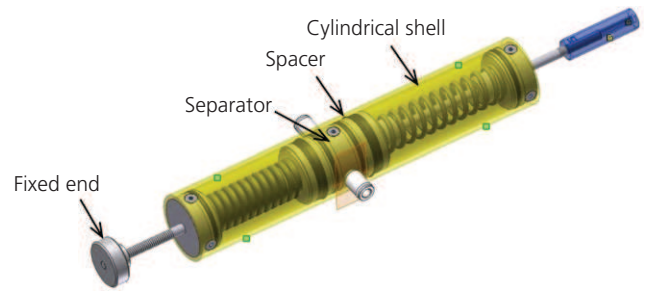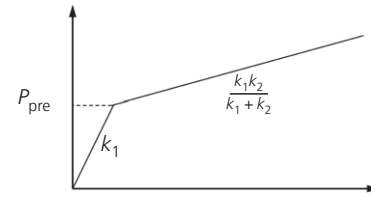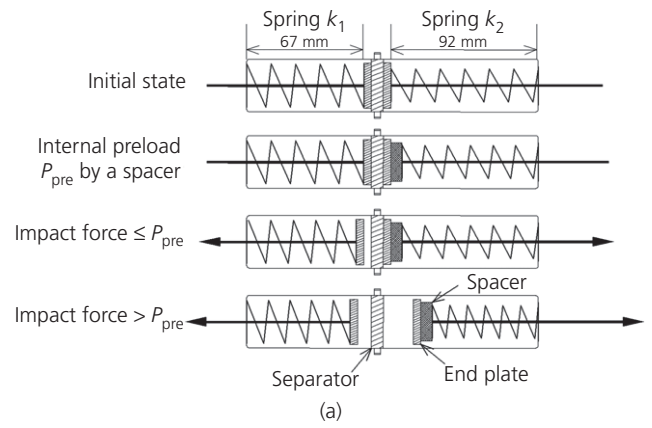
Fig. 2. Spring element: (a) simplified profile view; (b) bilinear behaviour; (c) overall view

is less than or equal to P_{pre}, then only spring k_1 becomes externally loaded. However, once the applied tensile force in the spring element exceeds P_{pre}, then both springs k_1 and k_2 act in series and the spring element is loaded at a stiffness of $k_1k_2/(k_1 + k_2)$. The spring element can replicate a simplified bilinear prototype loading behaviour (Fig. 1).

Instrumentation
Load cells were installed along each horizontal cable of the flexible barrier to measure the induced axial force. Laser sensors (resolution of 0·2 mm) were used to capture the displacement of the springs. A sampling rate of 20 kHz was adopted. A high-speed camera with a sampling rate of 640 frames/s and a resolution of 1300 × 1600 pixels was used to capture the impact kinematics and to facilitate particle image velocimetry analysis (White *et al*., 2003; Take, 2015).

Centrifuge model set-up
Figure 3 shows a side view of the centrifuge package on the platform of the centrifuge at the Hong Kong University of Science and Technology (Ng *et al*., 2001). A slope (25°) with a channel width of 233 mm and length of 530 mm was installed inside the model container (1245 mm × 350 mm × 850 mm). The channel was formed using the Perspex of the model container and a partition wall. Thirteen photoconductive sensors were installed along the centreline of

2
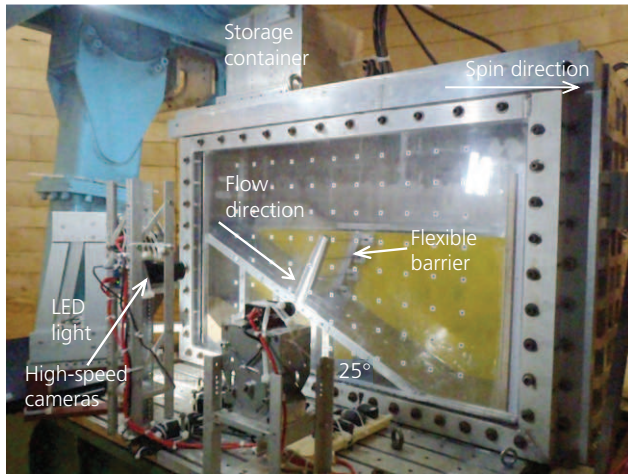
Fig. 3. Flexible barrier model set-up on centrifuge platform

Fig. 4. Flexible barrier model: (a) rigid post, plastic sheet and horizontal cables in front of the partition and (b) spring elements and instruments mounted on back of partition

the slope at intervals of 50 mm for the measurement of average frontal flow velocity. A storage container (0.03 m^3) was mounted over the upstream end of the slope to retain the debris. The storage container has a hinged door at the bottom. The opening of this hinged door (controlled using hydraulics) releases debris in-flight on to the channel.

A flexible barrier was installed perpendicular to the slope (Fig. 4(a)). A rigid post, 200 mm in height, was mounted on the slope and adjacent to the Perspex. The rigid post comprises ball and socket connections for each of the four horizontal steel strand cables (diameter of 3.3 mm). The four horizontal cables were uniformly distributed along the 200 mm barrier height and the bottom cable was in contact with the channel bottom. Such a simplification did not allow the debris to flow underneath the flexible barrier (Wendeler *et al.*, 2007). This represented a conservative loading scenario. The other end of each cable passed through the partition through a pulley system and attached to individual spring elements mounted on the back of the model container (Fig. 4(b)). Load cells were installed on each horizontal cable between the pulley and the spring element. Discs as reflectors were installed on the cable to allow displacement measurement using laser sensors (Fig. 4(b)). A plastic sheet, facilitating retention of debris, was applied along the upstream face of the flexible barrier to act as a net. Slack was provided in the sheet to ensure that under impact the sheet would stretch out and not be subjected to tension and the impact load would be fully transmitted to the horizontal cables.

QUASI-STATIC LOADING
Tension was applied to the spring element using an axial loading apparatus. The spring element parameters, namely k_1 (79.0 N/mm, model scale), k_2 (9.3 N/mm) and P_{pre} (80.0 N/mm), were determined by fitting a bilinear relationship through the measured prototype behaviour (Fig. 1).

The four spring elements exhibited the same loading responses. The spring element developed a bilinear loading behaviour and a distinct change in stiffness at the specified $P_{pre} = 40$ kN (prototype, Fig. 1) to simulate the energy-dissipating elements in a prototype barrier. A quasi-static loading test shows that the model stiffness could be less than the prototype at displacements less than 400 mm. The quasi-static loading response was set slightly lower than the prototype to allow for changes due to the inertial effect under high-*g* dynamic loading condition. Due to the inertial effect, a larger measured axial force was expected.
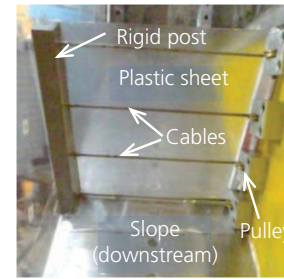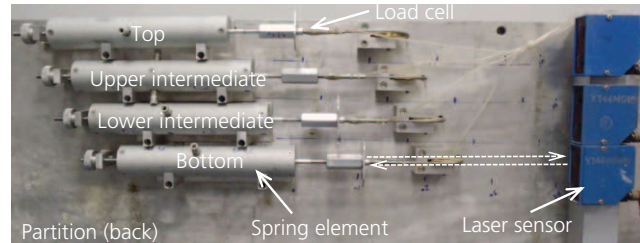
DYNAMIC GRANULAR IMPACT
Testing procedure
Dry Toyoura sand was adopted to verify the dynamic performance of the 200 mm high model barrier under $22.4g$ (nominal at $25g$). Dry sand measuring 0.022 m^3 was loaded in the model container. This is equivalent to 250 m^3 in prototype impacting a 4.5 m high and 4.5 m wide flexible barrier. After reaching $22.4g$, the debris was released on to the channel.

Captured kinematics
Figure 5 shows the observed loading sequence of dry sand on the model barrier captured using high-speed camera and its corresponding velocity fields. The time is defined that, at $t = 1.0$ s, the flow front reaches and impacts the barrier. The sand initially ran up along the base of the barrier and the flow velocity rapidly decreased from an initial frontal velocity of 11.7 to 5.8 m/s in about 0.5 s (Fig. 5(a)). Deposition, dead zone (Choi *et al.*, 2014) and subsequent laying occurred, and the flow velocity further attenuated (Figs 5(b) and 5(c)) before reaching a static state (Fig. 5(d)).

Measured axial load and displacement
Figure 6(a) shows the cable force–time evolution for each cable. As debris impacted the barrier, a rapid increase in loading of the bottom cable occurred and eventually reached P_{pre}. After this, a sudden drop in load was observed as the second spring was activated, corresponding to the activation of the energy-dissipating element in the prototype. The measured cable load fluctuated at the instant of activation of the energy-dissipating element. The rate of loading decreased as the impact process tends towards a static state. The delayed impact response of about 0.5 s between the bottom and the lower intermediate cable coincided with the observed pileup impact mechanism (Fig. 5). A flexible barrier is capable of transferring and redistributing impact load across the flexible barrier height, even to those areas non-intercepted debris. In Fig. 6(a), although debris physically reached 40% of the barrier height, the upper intermediate cable also bore impact load. The displacement of
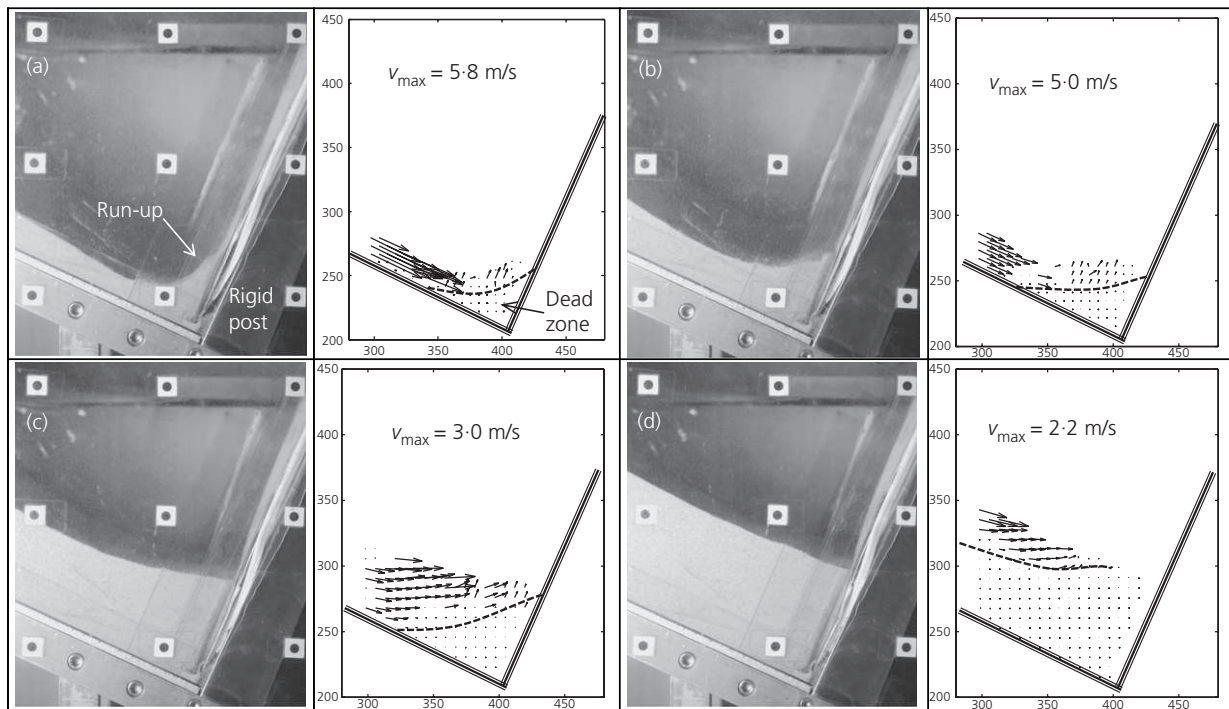
Fig. 5. Observed interaction kinematics in prototype time: (a) $t = 1 \cdot 56$ s; (b) $t = 1 \cdot 84$ s; (c) $t = 2 \cdot 40$ s; (d) $t = 2 \cdot 96$ s. The initial impact of dry sand started at $1 \cdot 0$ s
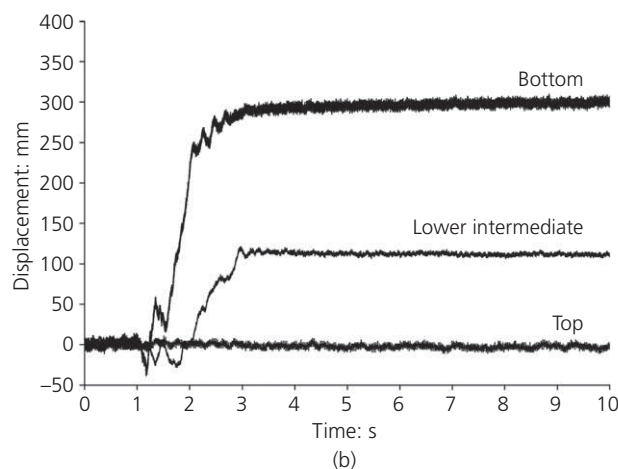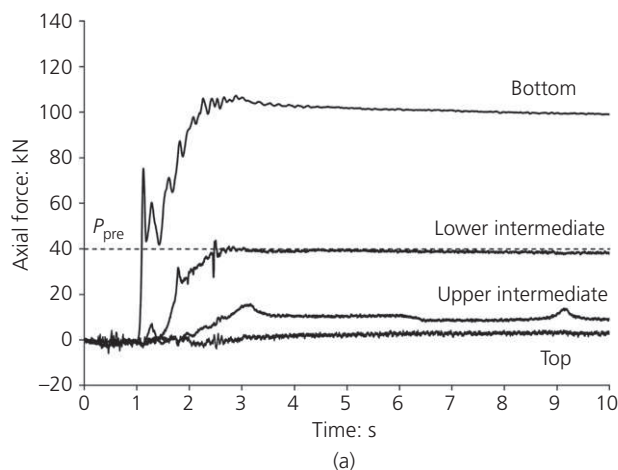
Fig. 6. High-**g** impact test: (a) cable force–time history and (b) cable elongation time history (all dimensions in prototype scale). Displacement for upper intermediate not measured due to limited working area on back of partition

each cable is shown in Fig. 6(b). The maximum elongation of the bottom cable is 300 mm in the prototype which was measured at the end of the test.

When comparing the dynamic response of the model barrier to static loading results and prototype conditions (Fig. 1), it is evident that the dynamic behaviour of the spring elements exhibited a steeper response during the initial stage of impact. Negative displacement could be attributed to the vibration of the cables during impact. The inflection point was higher in the dynamic test (about 50 kN) compared with the static preload P_{pre} (40 kN) due to the inertial effects of the barrier system. Although a higher than inflection point developed, the downscaled load–displacement behaviour of model barrier showed a reasonable agreement with the prototype behaviour.

Load attenuation mechanisms

Thick surge fronts were developed in the experiments of Ashwood (2014) by manually accelerating the sand using a paddle and those of Ishikawa *et al.* (2010) by using entrained bed load conditions. All these surge flow fronts showed high peak loads when they impacted the barriers. In contrast, the wedge-like granular impact front in this study developed a progressive pileup mechanism, without a distinct peak load (Fig. 6(a)). The influence of the flow front geometry is an important factor for the impact response of debris-resisting barriers.

In addition, the continuous deformation of the barrier led to load attenuation. As debris progressively deposited behind the barrier during impact, the incremental increase in lateral earth pressure triggered the elongation of the energy-dissipating devices. The lateral deformation of the flexible barrier in turn mobilised the internal strength of the deposited debris, allowing it to reach an active failure mode. This ensured a lower lateral earth pressure acting on the flexible barrier. The Coulomb earth pressure coefficient (k_a), for an inclined barrier and slope, is much higher than

4

that with vertical wall and flat ground. Given that the Toyoura sand has an internal friction angle of 31° (Ishihara, 1993) and an interface friction angle of 22·6° with the flexible barrier membrane (Choi et al., 2014), the calculated Coulomb k_a for a barrier inclined 25° downslope with a sloping surface of 30° is as high as 1·4. Based on the deduced load on the barrier, the earth pressure coefficient after the deposition is about 1·3, indicating an active mode. The barrier displaced subject to the debris impact. The displacement in turn led to the development of an active earth pressure, minimising the load acting on the barrier. The interactive mechanism between the displacement of the barrier and the reduction in earth pressure permits flexible barriers to retain more debris compared with rigid barriers where a k_o condition is usually assumed.

CONCLUSIONS

Details of a novel flexible barrier model for centrifuge modelling of landslide debris impact have been presented. Scaling laws of this model barrier were verified by the dynamic test results. The structural features of a flexible barrier facilitated the impact load transfer and redistribution along the barrier height. Compared with the peak loading behaviour induced by the impact of a surge front, the wedge-like flow front developed in this study, which is typical for dry granular flows, did not exhibit an obvious peak impact load. The continuous lateral displacement facilitated by the energy-dissipating devices ensured an active failure mode of dry sand and a reduced earth pressure acting on the barrier.

ACKNOWLEDGEMENTS

REFERENCES

Ashwood, W. (2014). Numerical model for the prediction of total dynamic landslide forces on flexible barriers. MASc thesis, The University of British Columbia, Vancouver, BC, Canada.

Bowman, E. T., Laue, J., Imre, B. & Springman, S. M. (2010). Experimental modelling of debris flow behaviour using a geotechnical centrifuge. Can. Geotech. J. 47, No. 7, 742–762.

Chan, S. L., Zhou, Z. H. & Liu, Y. P. (2012). Numerical analysis and design of flexible barriers allowing for sliding nodes and large deflection effects. In Proceedings of the one day seminar on natural terrain hazards mitigation measures, Hong Kong, pp. 29–43. The Association of Geotechnical and Geoenvironmental Specialists (Hong Kong) Limited, Hong Kong SAR.

Chi, K., Zakeri, A. & Hawlader, B. (2012). Impact drag forces on pipelines caused by submarine glide blocks or out-runner blocks. In Submarine mass movements and their consequences (eds Y. Yamada, K. Kawamura, K. Ikehara, Y. Ogawa, R. Urgeles, D. Mosher, J. Chaytor and M. Strasser), pp. 429–439. Dordrecht, the Netherlands: Springer.

Chikatamarla, R., Laue, J. & Springman, S. M. (2006). Centrifuge scaling laws for guided free fall events including rockfalls. Int. J. Phys. Model. Geotech. 6, No. 2, 15–26, http://dx.doi.org/10.1680/ijpmg.2006.060202.

Choi, C. E., Ng, C. W. W., Song, D., Kwan, J. H. S., Shiu, H. Y. K., Ho, K. K. S. & Koo, R. C. H. (2014). Flume investigation of landslide debris-resisting baffles. Can. Geotech. J. 51, No. 5, 540–553.

Ishihara, K. (1993). Liquefaction and flow failure during earthquakes. Géotechnique 43, No. 3, 351–451, http://dx.doi.org/10.1680/geot.1993.43.3.351.

Ishikawa, N., Inoue, R., Beppu, M., Hasegawa, Y. & Mizuyama, T. (2010). Dynamic load characteristics of debris flow model using different gravel size distribution. In Proceedings of INTERPRAEVENT (eds S. Chin and M. Mikoš), pp. 207–216. Taipei, Taiwan, R.O.C.: International Research Society INTERPRAEVENT.

Iverson, R. M. (1997). The physics of debris flows. Rev. Geophys. 35, No. 3, 245–296.

Iverson, R. M. (2015). Scaling and design of landslide and debris-flow experiments. Geomorphology 244, 9–20.

Kwan, J. S. H., Chan, S. L., Cheuk, J. C. Y. & Koo, R. C. H. (2014). A case study on an open hillside landslide impacting on a flexible rockfall barrier at Jordan Valley, Hong Kong. Landslides 11, No. 6, 1037–1050.

Nakai, T., Farias, M. M., Bastos, D. & Sato, Y. (2007). Simulation of conventional and inverted braced excavations using subloading t_{ij} model. Soils Found. 47, No. 3, 597–612.

Ng, C. W. W., Van Laak, P. A., Tang, W. H., Li, X. S. & Zhang, L. M. (2001). The Hong Kong geotechnical centrifuge. In Proceedings of the 3rd international conference on soft soil engineering (eds C. F. Lee, C. K. Lau, C. W. W. Ng, A. K. Kwong, P. L. R. Pang, J. H. Yin and Z. Q. Yue), pp. 225–230. Lisse: A.A. Balkema.

Take, W. A. (2015). Thirty-sixth Canadian geotechnical colloquium: advances in visualization of geotechnical processes through digital image correlation. Can. Geotech. J. 52, No. 9, 1199–1220.

Taylor, R. N. (ed.) (1995). Geotechnical centrifuge technology, 1st edn. Glasgow, UK: Blackie Academic Professional.

Volkwein, A., Schellenberg, K., Labiouse, V., Agliardi, F., Berger, F., Bourrier, F., Dorren, L. K. A., Gerber, W. & Jaboyedoff, M. (2011). Rockfall characterisation and structural protection – a review. Nat. Hazards Earth Syst. Sci. 11, 2617–2651.

Wendeler, C., McArdell, B. W., Rickenmann, D., Volkwein, A., Roth, A. & Denk, M. (2006). Field testing and numerical modeling of flexible debris flow barriers. In Proceedings of the sixth international conference of physical modelling in geotechnics (eds C. W. W. Ng, Y. H. Wang and L. M. Zhang), pp. 4–6. Boca Raton, FL, USA: CRC Press.

Wendeler, C., Volkwein, A., Denk, M., Roth, A. & Wartmann, S. (2007). Field measurements used for numerical modelling of flexible debris flow barriers. In Proceedings of fourth international conference on debris flow hazards mitigation: mechanics, prediction, and assessment (eds C. L. Chen and J. J. Major), pp. 681–687. Rotterdam, the Netherland: Millpress.

White, D. J., Take, W. A. & Bolton, M. D. (2003). Soil deformation measurement using particle image velocimetry (PIV) and photogrammetry. Géotechnique 53, No. 7, 619–631, http://dx.doi.org/10.1680/geot.2003.53.7.619.

Zhou, Z. H., Liu, Y. P. & Chan, S. L. (2011). Nonlinear finite element analysis and design of flexible barrier, Project Report. The Hong Kong Polytechnic University, Hong Kong SAR.